FEBS Letters

FEBS PRESS science publishing by scientists

RESEARCH LETTER

Engineering a highly sensitive biosensor for abscisic acid in mammalian cells

Seo Woo Kim[1,2,3,4], Kübra Alci[2,5], Femke Van Gaever[1,2], Yasmine Driege[1,2], Keylla Bicalho[6], Geert Goeminne[6], Claude Libert[1,2], Alain Goossens[3,4], Rudi Beyaert[1,2] and Jens Staal[1,2,7]

1 Center for Inflammation Research, VIB, Ghent, Belgium
2 Department of Biomedical Molecular Biology, Ghent University, Belgium
3 Center for Plant Systems Biology, VIB, Ghent, Belgium
4 Department of Plant Biotechnology and Bioinformatics, Ghent University, Belgium
5 BCCM/GeneCorner, Ghent University, Belgium
6 VIB Metabolomics Core Ghent, VIB, Ghent, Belgium
7 Department of Biochemistry and Microbiology, Ghent University, Belgium

Correspondence
J. Staal, Center for Inflammation Research, VIB, Technologiepark-Zwijnaarde 71, 9052, Ghent, Belgium
Tel: +32-9-3316765
E-mail: jens.staal@irc.vib-ugent.be

Alain Goossens, Rudi Beyaert and Jens Staal shared last authorship

(Received 3 January 2022, revised 21 May 2022, accepted 24 May 2022, available online 30 June 2022)

doi:10.1002/1873-3468.14431

Edited by Julian Schroeder

Abscisic acid (ABA) is a signalling molecule conserved in plants, bacteria, fungi, and animals. Recently, ABA has gained attention for its pharmacological activities and its potential as a biomarker for the severity of chronic obstructive pulmonary disease and glioma. This prompts the development of a reliable, sensitive, rapid, and cost-effective method to quantify ABA levels in mammalian cells and tissues. The previously described ABA biosensor system based on the ABA-dependent interaction between the plant ABA receptor PYL1 and co-receptor ABI1 is not sensitive enough for the low ABA levels seen in mammals. Therefore, we optimized this system by replacing PYL1 with other high-affinity plant PYL proteins. The optimized biosensor system engineered with the PYL8 receptor enabled the quantification of ABA at low concentrations in HEK293T cells.

Keywords: abscisic acid; biosensor; cell-based assay; synthetic biology

The development of biosensors enabled the characterization of various metabolites in many biological processes. Abscisic acid (ABA), a major phytohormone playing an essential role in plant abiotic stress responses, was one such metabolite whose dynamics were revealed in plants using biosensors based on the ABA signalling pathway in plants (Fig. 1A). For instance, to monitor ABA levels in different tissues of *Arabidopsis thaliana* L. in response to salinity or osmotic stress, a fluorescence resonance energy transfer (FRET)-based biosensor was used [1,2]. This biosensor translates the interaction between the ABA-induced conformationally rearranged the Pyrabactin Resistance 1 (PYR1)/PYR1-Like (PYL)/Regulatory Components of ABA Receptors (RCAR) ABA receptors, and the co-receptor protein phosphatases 2C (PP2C) (e.g., Abscisic acid Insensitive 1; ABI1) into fluorescence intensity [1,2]. In addition, other ABA-responsive reporter systems utilizing downstream ABA signalling components, such as the promoter region of ABA-responsive genes

Abbreviations
ABA, abscisic acid; COPD, chronic obstructive pulmonary disease; GAL4BD, GAL4 DNA-binding domain; HEK293T, Human Embryonic Kidney 293T; LANCL2, anthionine synthetase component C-like protein 2; PP2C, Protein Phosphatase 2C; PPARγ, Peroxisome proliferator-activated receptor gamma; PYL{1,8}, PYR1-like {1,8}; PYR1, Pyrabactin Resistance 1; RAR{α,β,γ}, Retinoic acid receptor {alpha, beta, gamma}; RCAR, Regulatory Components of ABA Receptors; SnRK2, snf1-related protein kinase 2; T2D, Type 2 diabetes; UAS, upstream activating sequence; VP16AD, VP16 transactivation domain.

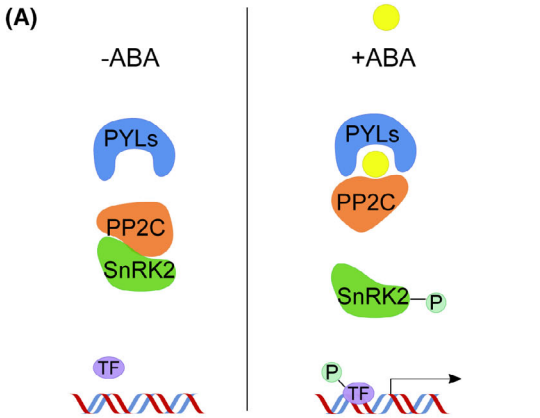

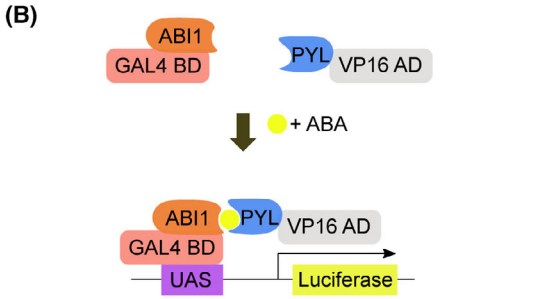

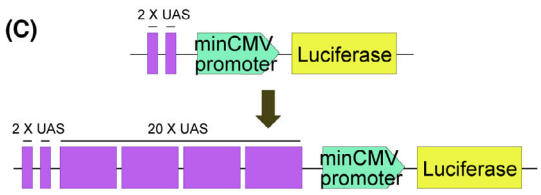

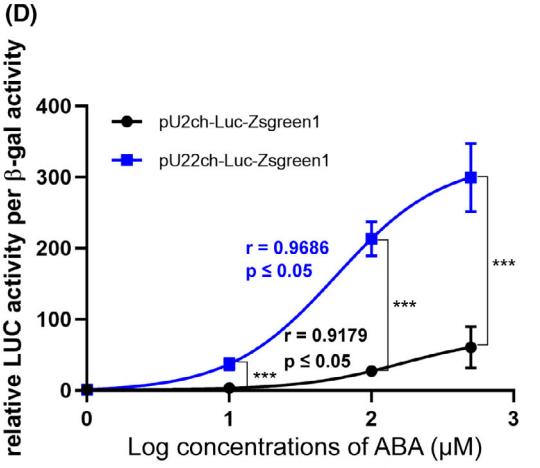

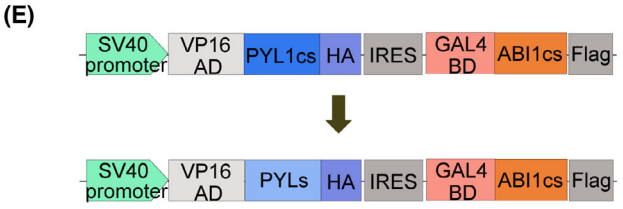

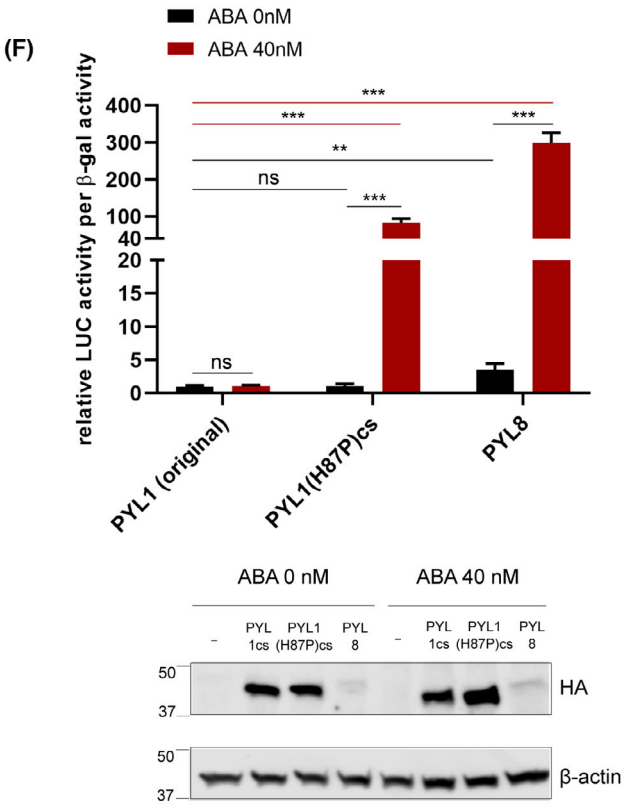

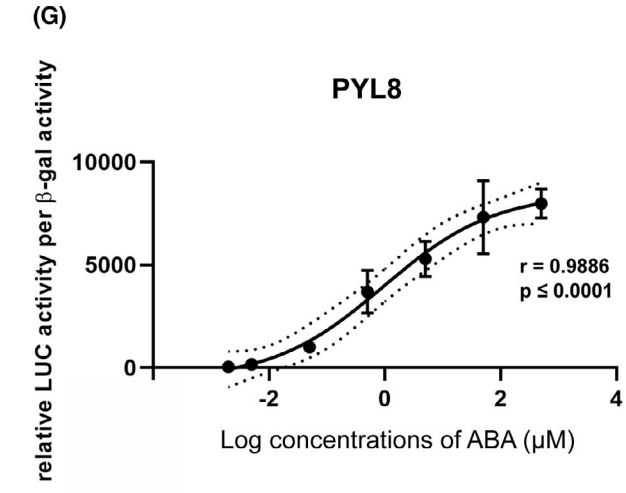

Fig. 1. Substitution of PYL1cs to PYL1 mutant and other PYL family receptors in the abscisic acid (ABA) biosensor construct alters ABA responsiveness. (A) Overview of the ABA signalling pathway in plants. A signalling complex composed of PYR/PYL/RCAR (PYL), protein phosphatases 2C (PP2C), and snf1-related protein kinase 2 (SnRK2) has been shown as a major component of the core ABA signalling cascade in plants. In the absence of ABA, PP2C negatively regulates SnRK2 activity. Once ABA levels increase in response to environmental stresses, ABA binding to the PYL receptor leads to the formation of an ABA–PYL–PP2C complex. SnRK2 is subsequently released from PP2C inhibition and thus activates downstream components such as ABA-responsive transcription factors by phosphorylation. (B) The underlying principle of the ABA-inducible luciferase assay system is based on the plant ABA core signalling pathway (figure adapted from [31]). ABA-dependent interaction between the plant ABA receptor PYL and the ABA co-receptor ABI1 brings the VP16AD to the GAL4-dependent promoter, leading to luciferase expression. (C) Generation of the custom UAS reporter constructs with 22 x UAS elements in the promoter region. (D) Comparison of the ABA-induced luciferase expression in HEK293T cells driven by two or 22 UAS repeats. HEK293T cells were transfected with the PYL1cs-based biosensor construct along with pACTβgal (normalization) and pU2CH-Luc-Zsgreen1 or pU22CH-Luc-Zsgreen1 (reporter) and incubated with ABA at the indicated concentrations. (E) Overview of the modifications made in the ABA biosensor construct. The complementary surfaces (CSs) of plant ABA receptor PYL1 in the original construct pSv-ABAactDA-PYL1 [31] were replaced with the hyperactive mutant PYL1 or different members of the PYL receptor family. Protein expression of HA-tagged PYL1, PYL(H87P), and PYL8 was analyzed by western blot analysis. β-Actin was used as a loading control. (F) Comparison of the ABA-induced luciferase expression in HEK293T cells expressing different PYL receptor-based biosensors. HEK293T cells were transfected with the indicated different PYL expression constructs along with pU22ch-Luc-Zsgreen1 and pACTβgal and incubated in the absence or presence of 40 nM ABA. (G) Dose–response curve for ABA in the ABA-inducible luciferase assay system utilizing the PYL8 receptor-based biosensor in HEK293T cells. Dotted lines represent 95% confidence intervals. HEK293T cells were transfected with the PYL8-based biosensor construct along with pU22CH-Luc-Zsgreen1 and pACTβgal and incubated with ABA at the indicated concentrations. Fold induction of ABA-induced luciferase expression in cells expressing the PYL receptor-based biosensor constructs is compared to the average background level of cells transfected with the empty vector. Luciferase values were normalized by β-galactosidase values. Error bars represent standard deviation (SD). Results are the means of four biological replicates and representative of two (F) or three (D, G) independent experiments. Each biological replicate refers to independent transfection. Statistical significance was calculated using a one-way ANOVA test (**P*-value ≤ 0.05, ***P*-value ≤ 0.01 and ****P*-value ≤ 0.001). *R*-value and *P*-value in (G) were calculated using simple linear regression analysis.

and the ABA-dependent kinase activity of snf1-related protein kinase 2 (SnRK2) family members, allowed deciphering ABA signal transduction as well as ABA homeostasis in plants [3–5].

Recent findings of the beneficial role of ABA administration in human clinical trials against type II diabetes (T2D) [6–10] and experimental animal models of several diseases, including inflammatory bowel disease [11,12], depression [13,14], and neuroinflammation [15,16], have proposed the potential use of ABA as a therapeutic or prophylactic agent for diseases of the metabolism-immune and gut-brain axes. Moreover, previous studies reported a difference in serum ABA levels between patients diagnosed with moderate and severe chronic obstructive pulmonary disease (COPD) [17], or between human high-grade and low-grade glioma tissues [18], suggesting ABA as a potential biomarker for the severity of these disorders.

Whereas ABA biosynthesis, catabolism, and signalling pathways are well known in plants, they are poorly understood in animals. A limited number of studies have proposed different mammalian ABA receptors [12,18–22]. First, lanthionine synthetase component C-like protein 2 (LANCL2), a peripheral membrane receptor, originally residing in the plasma membrane by N-terminal glycine myristoylation, translocates to the nucleus upon ABA binding [19]. Genetic depletion of LANCL2 specifically in muscle cells eliminates the protective effect of ABA in T2D, demonstrating its importance in an alternative insulin-independent blood sugar regulation mechanism [9]. A second demonstrated target of ABA is the nuclear receptor PPARγ, which is known to bind free fatty acids, the anti-diabetic drug rosiglitazone, and eicosanoids [20,23]. Previous studies showed that ABA activates PPARγ in a LANCL2-dependent manner [20,24]. Loss of PPARγ in immune cells is sufficient to block the protective effects from ABA in a model of colitis and diabetes [12,21], demonstrating that PPARγ regulates critical responses downstream of ABA. Several loss-of-function studies showed that PPARγ is necessary for the protective role of ABA against T2D, colitis, and influenza A virus infection [12,21,22]. Although ABA activates PPARγ, it does not bind to its known ligand-binding domain [20]. Finally, the retinoic acid signalling pathway was also shown to be involved in a potential inhibitory role of ABA in the pathogenesis of glioma [18]. mRNA expression levels of *RARβ* and *RARγ* were negatively correlated with the level of ABA in glioma tissue. A loss of function and the overexpression of RARα in U87-MG and A172 cells suggested that RARα positively impacts ABA-induced cancer cell apoptosis and differentiation [18]. Of note, retinoic acid and ABA share a similar structure since retinoic acid can be produced via cleavage of β-carotene in animals, which serves as a precursor in the plant ABA biosynthesis pathway [23].

Previous studies of ABA functions in mammals quantified ABA levels by enzyme-linked immunosorbent

assay (ELISA) and chromatography–mass spectrometry [25–28]. However, these analytical approaches have drawbacks. Both methods need sample extraction from mammalian tissues or cells, which limits the spatiotemporal resolution. In addition, ELISA is expensive, and its performance is highly influenced by antibody stability, thereby requiring appropriate transport and storage [29]. Tandem mass spectrometry, the most favorable chromatography–mass spectrometry for ABA in the context of sensitivity, is also expensive and requires complex protocols [30]. As an alternative approach, ABA-inducible reporter gene expression in cultured mammalian cells was developed [31]. This rapid and cost-effective system was engineered based on the ABA-dependent interaction of the plant ABA receptor PYL1 and the ABA co-receptor PP2C family member, ABI1 [31]. The complementary surfaces (CSs) of the PYL1 (PYLcs, amino acids 33–209) and the ABI1 (ABI1cs, amino acids 126–423, D143A mutant, lacking phosphatase activity) were fused to the VP16 transactivation domain (VP16AD) and GAL4 DNA-binding domain (GAL4BD), respectively (Fig. 1B). GAL4BD recognizes and binds to an upstream activating sequence (UAS), and VP16AD activates the general transcription factor machinery bound to the minimal promoter region of a downstream gene. In the presence of ABA, the PYL1cs/ABI1cs interaction therefore recruits VP16AD to the GAL4-dependent promoter and thus leads to the expression of a reporter gene (downstream of UAS) [31]. Unlike other measurement methods, this mammalian ABA-inducible system allows the extraction-free measurement of mouse serum or culture media [31]. Also, this system could enable monitoring ABA levels in ABA-producing cells and mouse in a spatial and/or temporal manner. Moreover, it has been used in various synthetic biology approaches for the design of on/off switches [32]. However, the detection limit of this system was shown to be relatively high (approximately 1 μM [31]), considering the low basal ABA levels in mammals (sub-nM concentrations) [1,33,34]. In addition, a reporter gene assay containing a peroxisome proliferator response element (PPRE) and PPARγ was previously used to evaluate the PPARγ activity upon ABA treatment [6,20]. However, this system only allowed the detection of ABA at a minimum of 1.25 μM. Therefore, this limitation establishes the need to engineer a novel sensitive ABA biosensor.

In this study, we optimized the above-described ABA biosensor system by replacing PYL1 with other plant PYL receptors displaying a higher affinity for ABA binding, which allowed the improvement of the sensitivity of the biosensor with a stronger signal-to-noise ratio. The ABA-dependent interaction between the PYL8 receptor and the co-receptor ABI1 in the optimized biosensor system allows the determination of ABA levels at low nM concentrations in HEK293T cells. Furthermore, the selectivity of the biosensor system for ABA was verified using the following ABA inactivation strategies: (1) the expression of a major *Arabidopsis* ABA 8′-hydroxylase *CYP707A3*, (2) the expression of anti-ABA single-chain Fv antibodies (scFv) in the endoplasmic reticulum (ER), and (3) the expression of *Arabidopsis* UDP-glucosyltransferase71C5 (*AtUGT71C5*).

Results and Discussion

Generation of a highly sensitive ABA biosensor based on the ABA-dependent interaction between the *Arabidopsis* PYL ABA-receptor and the co-receptor ABI1

To increase the sensitivity of the previously described ABA biosensor that is based on the GAL4DB-ABI1cs/VP16AD-PYL1cs-induced activation of a GAL4-dependent reporter gene [31] (Fig. 1B), we first added 20 extra repeats of the GAL4-dependent UAS to the original luciferase reporter construct (pU2CH-Luc-Zsgreen1), which only consisted of two tandem repeats of UAS in the old sensor system (Fig. 1C). Using the resulting 22 x UAS construct (pU22CH-Luc-Zsgreen1) caused a significant increase in the ABA-dependent luciferase reporter gene expression (Fig. 1D).

Next, we replaced PYL1 with other Arabidopsis PYL receptors displaying a higher apparent ABA-binding affinity. Compared to dimeric ABA receptors like PYL1, monomeric ABA receptors were reported to show higher ABA binding affinities [33]. For instance, altering dimeric PYR1 to monomeric PYR1 by a point mutation of a histidine 60 to proline (PYR1H60P) increased its apparent ABA affinity [33]. Likewise, a corresponding point mutation in PYL1 (H87P) in the above-mentioned FRET-based biosensor increased its affinity for ABA from $K_d \sim 80$ μM to $K_d \sim 2$ μM [1]. Therefore, we opted for the PYL1cs point mutation of histidine-87 to proline (pSv-ABAactDA-PYL1(H87P)) and another monomeric PYL8 (pSv-ABAactDA-PYL8), which will display a higher apparent affinity for ABA compared to PYL1 in the formation of the PYL–ABA–PP2C complex (Fig. 1E) [1,33,35,36]. Consistent with the previous report showing the higher affinity of PYL1(H87P) compared to PYL1 [1], the luciferase expression activated by ABA-induced interaction between PYL1 (H87P) and ABI1 was approximately 40-fold higher at 40 nM ABA in HEK293T cells than that driven by the

interaction between PYL1 and ABI1 in the presence of equimolar ABA (Fig. 1F).

The concentration-response curve for ABA-induced luciferase activation showed that the detection limit of the PYL8-based ABA biosensor in HEK293T cells was approximately 2–5 nM (Fig. 1G). It is worth noticing that ABA-untreated cells already exhibit a clear background signal (Fig. 1F). A previous study using a yeast two-hybrid assay showed that the interaction of PYL8 and another PP2C member hypersensitive to ABA 1 (HAB1) occurs in the absence of ABA [37], suggesting the spontaneous formation of a PYL8-ABI1 complex. Thus this background signal possibly reflects the ABA-independent formation of the PYL8-ABI1 complex. However, we are not aware whether these proteins spontaneously interact in mammalian cells which grow at a bit higher temperature (37 °C) compared to in plants or yeast. Another possible source for this background could be low amounts of endogenous ABA produced in HEK293T cells or ABA that is present in the serum of the cell culture medium (see also below). Together these data indicate that both PYL1(H87P)- and PYL8-based biosensor systems have enhanced sensitivity to ABA compared to the original PYL1-based biosensor.

ABA inactivation strategies validate the selectivity of the biosensor for ABA

To verify the selectivity for ABA of the improved PYL8-based biosensor, we applied the following ABA inactivation strategies: (a) the expression of a major *Arabidopsis* ABA 8′-hydroxylase AtCYP707A3 gene (pCS2-CYP7070A3-HA), (b) capturing ABA by expressing a gene encoding anti-ABA single-chain Fv antibodies (scFv) anchored to the endoplasmic reticulum (ER) with a C-terminal KDEL tag (pCS2-scFv-V5), and (c) the expression of *Arabidopsis* UDP-glucosyltransferase71C5 (AtUGT71C5) gene (pCS2-UGT71C5-myc).

In *Arabidopsis* ABA catabolism, the C-8′ position of ABA is predominantly hydroxylated by the cytochrome P450s (CYP), CYP707A1 to CYP707A4 [38]. CYP707A3 has been shown to catabolize ABA to phaseic acid in insect cells [39]. In agreement with this, the ABA-dependent luciferase expression significantly decreased in ABA-treated HEK293T cells expressing *AtCYP707A3* (Fig. 2A,B). Moreover, this depletion could be reversed by treatment of cells with the CYP707A inhibitor, abscinazole-E3M. The majority of CYP enzymes require the assistance of NADPH-cytochrome P450 reductase for the electron transfer from NADPH [40]. However, the overexpressed AtCYP707A3 depleted ABA in HEK293T cells without expressing additional CYP reductase, indicating the involvement of endogenous CYP reductase. The second strategy, anti-ABA scFv, was kindled by a previous study, showing that overexpression of ER-targeted anti-ABA scFv in tobacco results in an ABA-deficient phenotype [41]. Likewise, ABA-induced luciferase reporter expression in HEK293T cells was significantly less when anti-ABA scFv was overexpressed (Fig. 2C,D). Expression of an irrelevant transgene *NahG* (encoding an enzyme catalyzing the degradation of salicylic acid) under the same promoter and in an identical backbone vector (pCS2-NahG-V5), did not decrease luciferase expression in response to ABA. Finally, a third ABA depletion strategy, the expression of *Arabidopsis* UDP-glucosyltransferase71C5 (*AtUGT71C5*), has a role in ABA homeostasis in *Arabidopsis* through catalyzing ABA glucosylation [42], also significantly decreased ABA-induced luciferase expression in ABA-treated HEK293T cells (Fig. 2E,F). Transfection with the empty backbone vector plasmid (pCS2) did not lower ABA-induced luciferase activation. Taken together, these transgenic approaches validate the ABA selectivity of our newly developed PYL8-based ABA biosensor system.

The above-described experiments also show that all three ABA-inactivation methods, AtCYP707A3, anti-ABA scFv, and AtUGT71C5, significantly lower the background luciferase signal that is already observed in ABA-untreated HEK293T cells. This suggests that the background signal might derive from ABA that is present in the cell culture medium, or might be endogenous ABA produced in HEK293T cells. Since HEK293T cells show an adrenal and neuronal-like gene expression profile [43], and the brain is one of the most ABA-rich tissues in animals [27], endogenous ABA production by HEK293T cells is not so unlikely. However, as already mentioned above, this background signal may also result from the spontaneous formation of a PYL8-ABI1 complex. Our observation thus indicates that this background signal might be a combination of these two factors.

Evaluation of the use of human LANCL2, PPARγ, and RARs for the generation of novel ABA biosensors

LANCL2 was previously proposed as a mammalian ABA receptor [19,44]. PPARγ and RAR (α, β, γ) pathways have been linked to the anti-inflammatory activity of ABA and are also proposed as ABA receptors [12,18,20–22]. We therefore hypothesized the potential use of LANCL2, PPARγ, and RARs (α, β,

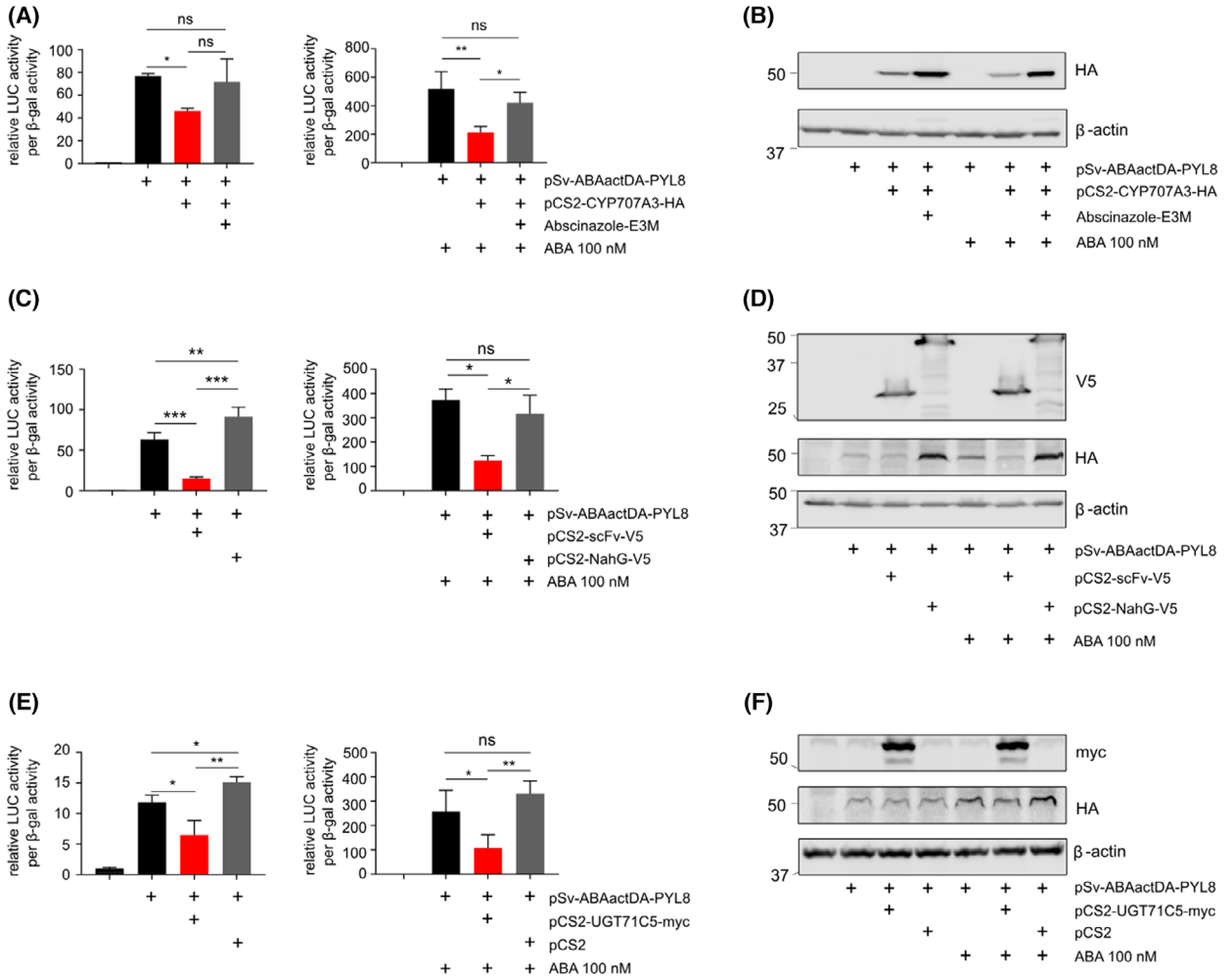

Fig. 2. Depletion of ABA in HEK293T cells upon overexpression of plant ABA catabolic genes or ABA-conjugating genes. (A) Effect of overexpression of *AtCYP707A3* on ABA-induced luciferase activity in HEK293T cells in the absence or presence of 10 μM of the CYP707A inhibitor abscinazole-E3M. Cells were transfected with the indicated construct along with the PYL8-based biosensor construct, pU22CH-Luc-Zsgreen1 and pACTβgal, and incubated in the presence or absence of 100 nM ABA or 10 μM abscinazole-E3M. (B) Western blot analysis of protein expression of HA-tagged CYP707A3. Protein expression of HA-tagged VP16AD-PYL8 could not be verified due to the high accumulation of HA-tagged CYP707A3 with similar molecular weight (50 kD). (C) Effect of overexpression of *anti-ABA scFv* on ABA-induced luciferase activity in HEK293T cells. Cells transfected with the irrelevant transgene NahG carried in the same backbone vector as anti-ABA scFv were used as a negative control. HEK293T cells were transfected with the indicated construct along with the PYL8-based biosensor construct, pU22CH-Luc-Zsgreen1 and pACTβgal, and incubated in the presence or absence of 100 nM ABA. (D) Western blot analysis of protein expression of V5-tagged scFv and NahG and HA-tagged VP16AD-PYL8. (E) Effect of overexpression of *AtUGT71C5* on ABA-induced luciferase activity in HEK293T cells. Cells transfected with the control backbone empty vector (EV) plasmid (pCS2) were used as a negative control. (F) Western blot analysis of protein expression of Myc-tagged UGT71C5 and HA-tagged VP16AD-PYL8. Fold induction of ABA-induced luciferase expression in cells expressing the PYL8 receptor-based biosensor construct is compared to the average background level of cells transfected with the empty vector. Luciferase values were normalized by β-galactosidase values. β-Actin was used as a loading control. Error bars represent SD. Results are the means of three biological replicates and are representative of at least two independent experiments. Each biological replicate refers to independent transfection. Statistical significance was calculated using a Home-Sidak's multiple comparisons test (pairwise): **P*-value ≤ 0.05, ***P*-value ≤ 0.01 and ****P*-value ≤ 0.001.

γ) for the generation of a novel GAL4-VP16/UAS driven ABA biosensor [12,18–22,44].

LANCL2 is anchored in the cell membrane via myristoylation. Translocation of LANCL2 from the membrane to the nucleus upon binding to ABA has been suggested to result from the loss of myristoylation at the N-terminus [19]. We therefore fused the GAL4BD-VP16AD to the C-terminus of LANCL2

(Fig. 3A,B), and hypothesized that the membrane-anchored LANCL2-GAL4BD-VP16AD would translocate to the nucleus upon ABA treatment in HEK293T cells, subsequently transactivating luciferase reporter gene expression. However, luciferase expression was already activated in untreated cells expressing such as LANCL2-GAL4BD-VP16AD fusion protein and did not further increase upon ABA treatment. We observed the accumulation of LANCL2-GAL4BD-VP16AD protein in nuclear fractions of untreated cells (Fig. 3C). The nuclear localization sequence that is present in GAL4BD thus overcomes the effect of myristoylation-mediated membrane anchoring, resulting in the ABA-independent nuclear translocation, which invalidates such an approach.

PPARγ and RARs (α, β, γ) are nuclear hormone receptors that elicit transcription-activating functions [45,46]. Hypothesizing their activation by ABA, we therefore fused the GAL4BD to each of these nuclear receptors and measured the expression of a GAL4-dependent luciferase reporter gene in HEK293T cells transfected with the corresponding GAL4BD-PPARγ, GAL4BD-RARα, Gal4BD-RARβ, and GAL4BD-RARγ expression plasmids (Fig. 3A,B). Treatment with the PPARγ-ligand rosiglitazone and the RAR-ligand retinoic acid were used as positive controls. However, ABA treatment did not induce GAL4BD-PPARγ or GAL4BD-RARs (α, β, γ)-dependent luciferase activity (Fig. 3D–G), nor did ABA affect luciferase gene expression induced by the known RAR and PPARγ ligands (Fig. 3D–G). Therefore, these results demonstrate that the construction of an ABA biosensor based on PPARγ and RAR is not a valid approach.

It has been reported that PPARγ is activated indirectly by ABA in a LANCL2-dependent manner [20,24]. To our surprise, in HEK293T cells, the PPRE-based reporter gene assay showed that the endogenous level of LANCL2 was sufficient to activate PPARγ activity [24]. In addition, it is still completely unknown how the RAR signalling pathway is implicated in the physiological function of ABA. A better understanding of ABA signalling pathways associated with PPARγ activation and the regulation of RARs will be essential in the further engineering of ABA-dependent cell-based assays utilizing these receptors.

Applications and future perspectives

Recent advanced knowledge of ABA as a therapeutic/prophylactic agent and a biomarker for the severity of certain disorders such as COPD and glioma prompted the need for a reliable, sensitive, economical, and rapid ABA quantification method. In the present study, we improved the sensitivity of a previously described ABA biosensor system by employing a PYL1(H87P) or PYL8–ABA–PP2C ternary complex of *Arabidopsis* ABA signalling, which allows the quantification of ABA at levels down to low nM concentration in HEK293T cells. Applying three different ABA inactivation strategies using AtCYP707A3, anti-ABA scFv, and AtUGT71C5, validated the selectivity of the ABA biosensor system.

Liang et al., demonstrated the measurement of ABA in serum of mice orally given with ABA [340 mg·kg^{-1} body weight (BW)] using the original PYL1-based system, which showed its therapeutic application. However, the ABA dose of 340 mg·kg^{-1} BW is relatively high compared to the dose used for the therapeutic/prophylactic treatment [22]. We thus examined whether our improved biosensor could detect ABA levels in mice treated with the dose of ABA close to the therapeutic level (100 mg·kg^{-1} feed), which was opted for several studies investigating the effect of ABA in a mouse model of colitis [15–17], atherosclerosis [28], and systemic inflammation (lipopolysaccharide model) [29]. We were able to detect ABA in serum of mice given ABA-supplemented diets for 7 days, which was also confirmed by liquid chromatography–mass spectrometry analysis (LC–MS) (Fig. 4A,B). It should however be noted that both measurements came from different mice that underwent the same treatment so no direct comparison between the two methods can be done with regards to relative sensitivity. The two non-responders in the LC–MS group could either be due to individual variation since the ABA is given via *ad libithum* feeding or due to loss in the pre-processing steps of ABA (extraction, purification, and concentration) in the LC–MS analysis. Those preprocessing steps were not needed for the bioassay where serum was added directly to the cells. We believe that both methods have further room for improvement, with further modifications to the bioassay to increase the signal/noise ratio at low ABA concentrations and the LC–MS analysis could potentially be further improved by optimizing the preprocessing of the material.

In this study, HEK293T cells were used to validate our engineered ABA biosensor system due to its straightforward transfection with high efficiency. Along with genetic [e.g., small interfering RNA (siRNA) and clustered regularly interspaced short palindromic repeats (CRISPR)/CRISPR-associated protein 9 (CRISPR/Cas9)] or pharmacological means, it could also be a powerful tool to screen for molecular and cellular mechanisms that regulate mammalian ABA metabolism also in other cell types. For example, RAW264.7 cells can be an interesting model, given the

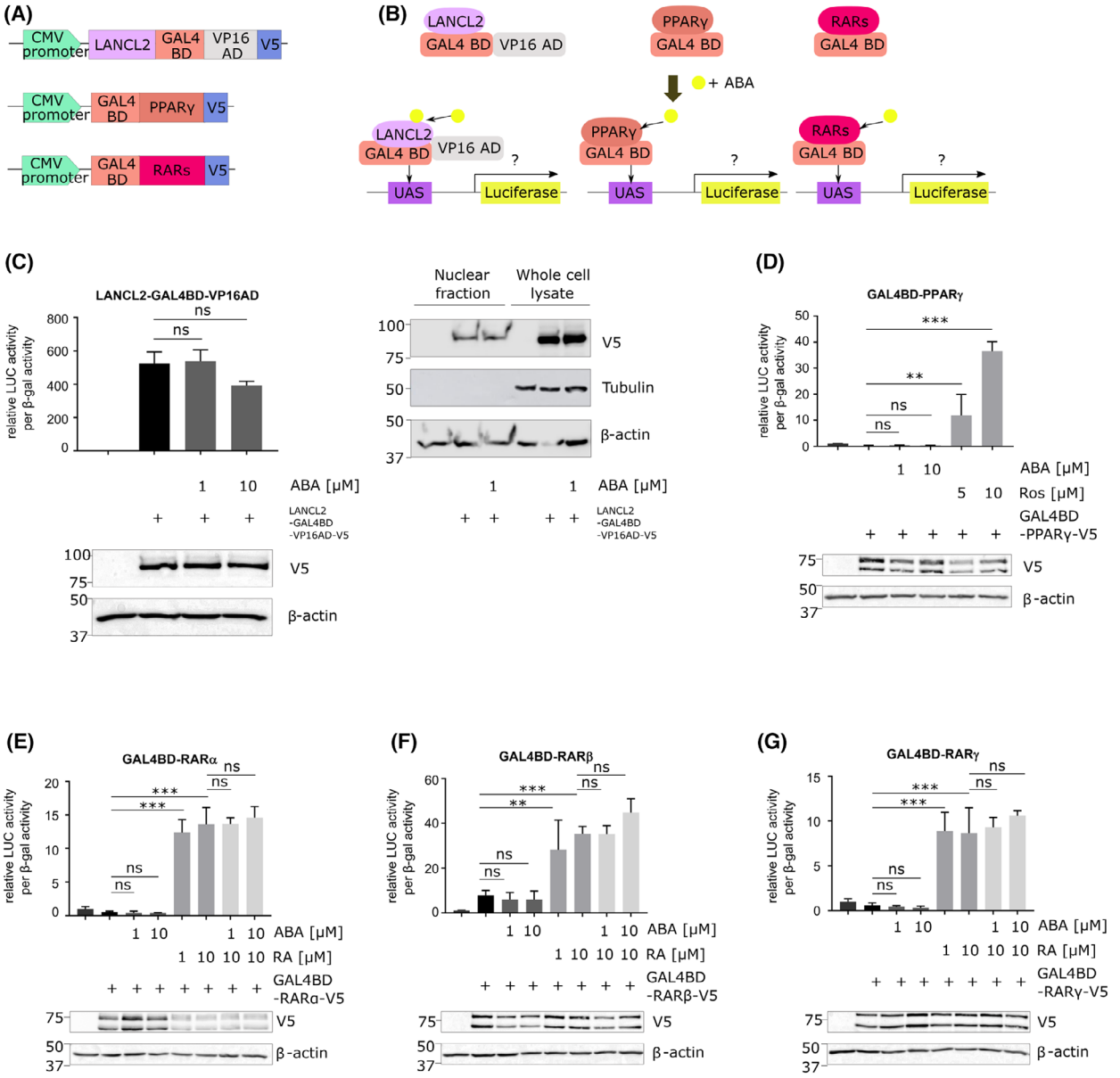

Fig. 3. Evaluation of potential human ABA receptors in HEK293T cells. (A) Overview of the different GAL4DB fusion proteins of potential human ABA receptors whose expression is driven by the CMV promoter. The V5 epitope tag is fused to monitor the receptor protein expression via western blotting. (B) The underlying principle of the ABA-inducible luciferase assay is based on the proposed role of different human ABA receptors. (C, D) Luciferase activity in HEK293T cells containing the pU22CH-Luc-Zsgreen1 reporter construct. HEK293T cells were co-transfected with the LANCL2-GAL4BD-VP16AD (C) or GAL4BD-PPARγ (D) expression constructs along with pACTβgal (used for normalization of transfection efficiency) and incubated with ABA or rosiglitazone (Ros). Protein expression of V5-tagged nuclear or total cellular LANCL2-GAL4BD-VP16AD or GAL4BD-PPARγ was verified by western blot analysis. (E–G) Analysis of RARα- (E), RARβ- (F), RARγ (G)-dependent luciferase expression in HEK293T cells containing the pU22CH-Luc-Zsgreen1 reporter construct. HEK293T cells were co-transfected with the corresponding fusion protein GAL4BD-RARs expression constructs along with pACTβgal and incubated with ABA or retinoic acid (RA). Protein expression of V5-tagged GAL4BD-RARs was verified by western blot analysis. The lower molecular weight immunoreactive band among two distinct bands might be due to an alternative translation site. Fold induction of luciferase expression in cells expressing *LANCL2*, *PPARγ*, or *RARs* is compared to the average background level of cells transfected with the empty vector. Luciferase values were normalized by β-galactosidase values. Tubulin was used as a cytoplasmic fraction control. β-Actin was used as a loading control. Error bars represent SD. Results are the means of four biological replicates and are representative of two independent experiments. Each biological replicate refers to independent transfection. Statistical significance was calculated using a one-way ANOVA test (**P*-value ≤ 0.05, ***P*-value ≤ 0.01 and ****P*-value ≤ 0.001).

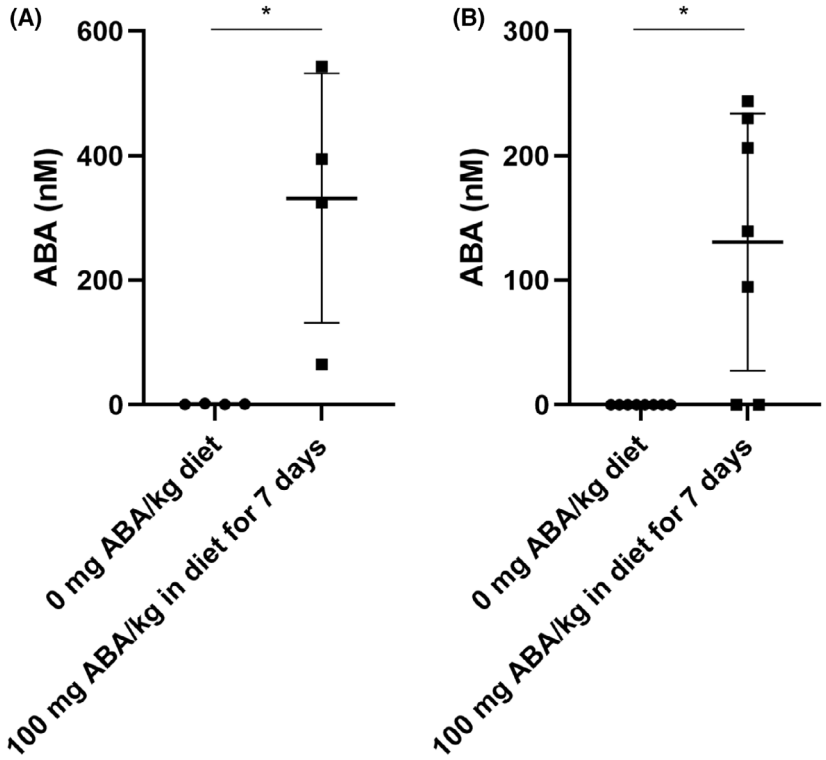

Fig. 4. ABA measurement in serum from mice given an ABA-supplemented diet. ABA measurement in serum from mice given control diets or ABA-supplemented diets (100 mg·kg^{-1}) for 7 days by PYL8 biosensor (A) and liquid chromatography–mass spectrometry (Vion IMS QTof mass spectrometer analysis) (B). HEK293T cells were transfected with the PYL8-based biosensor construct along with pU22CH-Luc-Zsgreen1 and pACTβgal and incubated with serum. Fold induction of ABA-induced luciferase expression in cells expressing the PYL receptor-based biosensor constructs is compared to the average background level of cells transfected with the empty vector. Luciferase values were normalized by β-galactosidase values. Error bars represent standard deviation (SD). Data shown are from one experiment. Each dot represents one mouse. ABA levels in each mouse range from 0 to 600 nM as individual food intake and metabolism can not be controlled and monitored in *ad libitum* feeding. Serum ABA concentrations were estimated based on a standard curve made with mouse serum spiked with known amounts of ABA. Statistical significance was calculated using a one-way ANOVA test (*P-value ≤ 0.05, **P-value ≤ 0.01 and ***P-value ≤ 0.001).

inhibiting effect of ABA against LPS-induced inflammation response and the increased level of ABA in response to quartz particles [4,5]. Moreover, our biosensor system could be used like ELISA to quantify ABA levels in the culture supernatant of a wide range of cell types under various physiological conditions. For instance, β-cell-like rat insulinoma cells (INS-1) are shown to secrete ABA upon glucose treatment, which might induce insulin release and glucose uptake by muscle and adipose tissue [47,48]. A recent immortalized mouse β-cell line (MIN-CB4) [49] could be highly interesting for the genetic characterization of ABA biosynthesis since there are more genetic tools like CRISPR and RNAi libraries for mice. To reveal whether endogenous ABA plays a role in the interplay between inflammation and glucose or lipid metabolism, one could stimulate β-cells with adipokines (e.g., adiponectin) or inflammatory cytokines [e.g., tumor necrosis factor (TNF)-α, interleukin (IL)-1β, and IL-6] and assess their extracellular ABA levels using our biosensor system in HEK293T cells [50].

Synthetic biology studies have used the PYL1–ABI1 complex formation as they can predictably and orthogonally modulate cellular processes in mammalian cells without disturbing the host's natural biological system [32]. These synthetic biology approaches can also benefit from our improved sensitivity for ABA in the biosensor with different PYL variants. Given that the PYL8-based biosensor exhibits a background (exogenous) ABA-independent signal output, the sensitive PYL1(H87P) is probably a better choice for those use cases since it shows a low background in the absence of exogenous ABA. We also envision that the improved ABA biosensor could contribute to large-scale studies that require the quantification of ABA as a biomarker in biological samples in the context of

clinical application. Altogether, our improved ABA biosensor system will help future studies define the physiological role and metabolism of ABA, which might bring new therapeutic approaches.

Material and methods

Modification and construction of ABA biosensors

pSv-ABAactDA (pSV40-VP16AD-PYL1cs-HA-IRES-GAL4BD-ABI1-Flag) was a gift from Dr. J. Crabtree (Standford University, USA, Addgene plasmid no. 38247) via Addgene (https://www.addgene.org) [31] and was modified to obtain variants (Table 1). H87P mutation in the *PYL1* gene in pSv-ABAactDA was generated by PCR mutagenesis (see Table 2 for primers used). *PYL8* CDS was amplified from *Arabidopsis* cDNA using indicated primers. The PCR products were cloned between *Asc*I and *BamH*I into the pSv-ABAactDA plasmid, from which *PYL1* was removed. All constructs were verified by Sanger sequencing. All plasmids generated in this study were deposited in the BCCM/GeneCorner plasmid collection (https://www.genecorner.ugent.be/).

To generate pLenti6-LANCL2-GAL4BDVP16AD-V5, *LANCL2* was amplified from pET28b-LancL2 (a gift from Jie Chen, the University of Illinois at Urbana-Champaig, USA, Addgene plasmid no. 73407) (https://www.addgene.org/), and the PCR product was subsequently cloned into pDNOR201 by Gateway BP clonase reactions according to manufacturer's instructions (Invitrogen, Carlsbad, CA, USA).). To generate pLenti6-GAL4BD-PPARγ-V5, pLenti6-GAL4BD-RARα-V5, pLenti6-GAL4BD-RARβ-V5, and pLenti6-GAL4BD-RARγ-V5, ORFs of *PPARγ, RARα, RARβ, and RARγ*, respectively, cloned in pENTR223 from Human ORFeome library v8.1 were used [51]. These receptors were subsequently transferred into the expression vector pLenti6-V5-puro by Gateway LR clonase reactions (Invitrogen). *GAL4BD-VP16AD* and *GAL4BD* were amplified from pGal4-VP16 using indicated primers (Table 2). To generate the final constructs, the *GAL4BD-VP16AD* PCR product was cloned into *XhoI*-opened pLenti6-LANCL2-V5 for C-terminal fusion, and the *GAL4BD* PCR product was cloned into *SpeI*-opened

Table 1. Overview of plasmids used in this study. Plasmids were deposited in the BCCM/GeneCorner plasmid collection (https://www.genecorner.ugent.be/).

Plasmid name	Source	BCCM/GeneCorner accession number
pSV-ABAactDA-PYL1	[31]	(Addgene plasmid no. 38247)
pSv-ABAactDA-PYL1(H87P)	This study	LMBP 11274
pSv-ABAactDA-PYL8	This study	LMBP 11503
pET28b-LanCL2	[52]	(Addgene plasmid no. 73407)
pENTR223-PPARγ	[51]	LMBP ORF81087-A06
pENTR223-RARα	[51]	LMBP ORF81085-F08
pENTR223-RARβ	[51]	LMBP ORF81093-C07
pENTR223-RARγ	[51]	LMBP ORF81123-C12
pDNOR201-LANCL2	This study	LMBP 12461
pLenti6-V5-puro	[53]	LMBP 09590
pGal4-VP16	[54]	LMBP 4708
pLenti6-LANCL2-GAL4BD-VP16AD-V5	This study	LMBP 12804
pLent6-GAL4BD-PPARγ-V5	This study	LMBP 12805
pLenti6-GAL4BD-RARα-V5	This study	LMBP 12806
pLenti6-GAL4BD-RARβ-V5	This study	LMBP 12807
pLenti6-GAL4BD-RARγ-V5	This study	LMBP 12808
pU2CH-Luc-Zsgreen1	This study	LMBP 11219
pENTR-L1-20 × UAS-L4	[55]	(Addgene plasmid no. 32307)
pU22CH-Luc-Zsgreen1	This study	LMBP 11226
pACTβgal	[56]	LMBP 4341
pUC19-BamHI-VSV-mAtCYP707A3-HA-P2A-ZsGreen-XhoI	This study	LMBP 9631
pENTR3C-VSV-mAtCYP707A3-P2A-ZsGreen1	This study	LMBP 9660
pCS2-VSV-mAtCYP707A3-HA	This study	LMBP 9909
pUC57-SP-scFv(ABA)-V5-KDEL	This study	LMBP 10803
pENTR3C-SP-scFv(ABA)-V5-KDEL	This study	LMBP 10805
pCS2-SP-scFv(ABA)-V5-KDEL	This study	LMBP 10807
pCS2-nahG-V5	This study	LMBP 10808
pEF6-AtUGT71C5-myc/his	This study	LMBP 9823
pEF6/Myc-HisA	Invitrogen	(commercial plasmid)

Table 2. Overview of primers and oligonucleotides used in this study. Bold text indicates restriction enzyme sites induced by PCR.

	Sequence
PYL1-H87P-F	taggccacagatttacaaacccttcatcaaaagctgtaacg
PYL1-H87P-R	cgttacagcttttgatgaagggtttgtaaatctgtggccta
*Asc*I-PYL8-F	cagtg**ggcgcgcc**atggaagctaacgggattga
PYL8-HA-*BamH*I-R	cgat**ggatcc**tcaagcgtaatctggaacatcgtatgggtagactctcgattctgtcgtgt
attB1-LANCL2-F	ggggacaagtttgtacaaaaaagcaggctatgggcgagaccatgtcaaaga
attB2-LANCL2-R	ggggaccactttgtacaagaaagctgggttttgtcatcgtcatccttagtgtcatcc ctcttcgaagagtcaagttca
GAL4BD-F-clonez	gactctagaggatccactagtatgaagctactgtct
GAL4BD-R-clonez	attccaccacactggatcgatacagtcaactgt
GAL4BD-VP16AD-F-clonez	gcacagtggcggccgttatgaagctactgtcttct
GAL4BD-VP16AD-R-clonez	ccgcgggccctctagattcccaccgtactcgtcaat
*Spe*I-pU2CH-LucZsGreen-F	caca**actagt**tatgtcgaggtggcgtgtacggtgg
*Kpn*I-pU2CH-LucZsGreen-R	gcct**ggtacc**gactacagtactccgctc
*Kpn*I-20xUAS-F	tagtc**ggtacc**gagcaatgcttttttataatgcc
*Xba*I-20xUAS-R	acac**tctaga**gccaactttgtatagaaaagttggg
*Kpn*I-AtUGT71C5-F	acat**ggtacc**atgaagacagcagagctcatattcg
*Spe*I-AtUGT71C5-R	gtaa**actagt**aaagtgatccccaagaatatctttg

pLenti6-PPARγ-V5, pLenti6- RARα-V5, pLenti6-RARβ-V5, and pLenti6-RARγ-V5 for N-terminal fusion using NEBuilder HiFi DNA Assembly master mix according to manufacturer's instructions (New England BioLabs, Ipswich, MA, USA).

To generate pU22CH-Luc-Zsgreen1 (i.e., 22 × UAS), first, pU2CH-Luc-Zsgreen1 (i.e., 2 × UAS) was linearized and extended with *SpeI* and *KpnI* by PCR. Second, the 20 × UAS sequence was amplified from pENTR-L1-20 × UAS-L4 (a gift from S. Stowers, Montana State University, USA, Addgene plasmid no. 32307) using indicated primers (Table 2). Finally, the 20 × UAS PCR product was subsequently cloned into *SpeI*- and *KpnI*- opened pU2CH-Luc-Zsgreen1, generating pU22CH-Luc-Zsgreen1.

Construction of vectors for the expression of ABA-catabolic genes or ABA-conjugating genes

HA-tagged mouse codon-optimized ABA-degrading P450 *AtCYP707A3* was synthetically generated and cloned into a pUC19 vector (Genscript, Leiden, The Netherlands). pUC19-VSV-mAtCYP707A3-HA-P2A-ZsGreen was digested with *BamHI* and *XhoI* and ligated with *BamHI*- and *XhoI*-opened pENTR3C vector. A Gateway LR clonase reaction was performed to transfer an HA-tagged VSV-mAtCYP707A3 construct into a pCS2 vector according to the manufacturer's instructions (Invitrogen, Waltham, MA, USA).

Mouse codon-optimized small single-chain antibody against ABA with secretion tag (SP) and ER retention tag (KDEL) for intracellular expression was also synthetically generated and cloned into a pUC57 vector (Genscript). An SP-scFv-V5-KDEL construct was cloned into *BamHI*- and *XbaI*-opened pENTR3C vector. A Gateway LR clonase reaction was performed to transfer an SP-ScFv-V5-KDEL construct into a pCS2 vector according to the manufacturer's instructions (Invitrogen). *AtUGT71C5* was amplified from *Arabidopsis* genomic DNA using indicated primers (Table 2) and cloned into *KpnI*- and *SpeI*-opened pEF6/myc-His vector.

Cell culture and transfection

HEK293T cells were cultured in Dulbecco's Modified Eagle Medium (DMEM) from Gibco (Waltham, MA, USA), supplemented with 10% fetal bovine serum. HEK293T cells were seeded at a density of 4×10^4 cells in 24-well plates and transfected with a total of 250 ng of plasmid DNA per well using a calcium phosphate method. pACTβgal (a gift from Dr. J. Inoue, Institute of Medical Sciences, Tokyo, Japan) encoding β-galactosidase was co-transfected in each well as an internal control. In addition to a luciferase reporter plasmid and vectors encoding genes of interest, an empty vector was added to maintain equal amounts of DNA in each transfection. Six hours after transfection, the medium was refreshed with or without the addition of ABA (A4906, Sigma, St Louis, MO, USA) and CYP707A inhibitor abscinazole-E3M and incubated overnight at 37 °C/5% CO_2. Abscinazole-E3M was a gift from Dr. Y. Todoroki (Shizuoka University, Japan) [46]. As controls to validate the transcriptional activity of GAL4BD-PPARγ and GAL4BD-RARs, Rosiglitazone (R2408, Sigma) and Retinoic acid (R2625, Sigma) were added to cells at the indicated concentrations when the medium was refreshed 6 h after the transfection.

ABA-inducible luciferase assay

The transfected HEK 293T cells were lysed in luciferase lysis buffer (25 mM Tris-phosphate pH 7.8, 2 mM DTT,

2 mM CDTA, 10% glycerol, 1% Triton X-100). To cell lysates, D-luciferin (E1605, Promega, Madison, WI, USA) and CPRG substrate (10884308001, Sigma) dissolved in CPRG buffer (60 mM Na_2HPO_4, 10 mM KCl, 1 mM β-mercaptoethanol) were added respectively. Luminescence signals were measured using the GloMax® 96 Microplate Luminometer (Promega), and β-galactosidase activity was quantified using the iMark™ microplate reader (Biorad, Hercules, CA, USA) at a wavelength of 595 nm. To correct variations in transfection efficiency, luciferase values were normalized by β-galactosidase values.

Immunoblotting

The expression of receptors and ABA-inactivating proteins was confirmed by immunoblotting. 5× Laemmli buffer (250 mM Tris–HCl, pH 8, 10% SDS, 50% glycerol, 0.005% bromophenol blue, 25% β-mercaptoethanol) was added to cells lysed in RIPA buffer (50 mM Tris–HCl, pH 7.6, 1 mM EDTA, 150 mM NaCl, 1% NP-40, and 0.5% sodium deoxycholate, 0.1% SDS) with protease and phosphatase inhibitors, followed by denaturation for 10 min at 95 °C. Proteins were separated by 10% SDS/PAGE, transferred to nitrocellulose membranes with 0.45 μm pores (Protran, Perkin Elmer, Waltham, MA, USA), and probed with the following specific antibodies: anti-HA.11 (MMS-101R-B, Babco, Antwerp, Belgium), anti-myc (PEPcore, Ghent, Belgium), anti-V5-HRP (R96125, Invitrogen), anti-Tubulin (T4026, Sigma) anti-β-actin-HRP (sc-47 778, Santa Cruz, Dallas, TX, USA), and anti-mouse IgG secondary antibody conjugated to HRP (31432, Thermo Fisher Scientific, Waltham, MA, USA). Western Lightning ECL detection system (Perkin Elmer) was used for protein detection according to the manufacturer's instructions.

Nuclear fractionation

To separate nuclear fractions, B1 buffer (10 mM HEPES pH 7.5, 10 mM KCl, 1 mM $MgCl_2$, 5% glycerol, 0.5 mM EDTA pH 7.5, 0.1 mM EGTA pH 7.5, 0.5 mM DTT) with protease and phosphatase inhibitors was added to cells, followed by resuspension and incubation for 15 min at 4 °C. 10% NP-40 buffer was added, and cell lysates were briefly vortexed. Next, the lysates were further centrifuged at 10 600 ***g*** for 15 min at 4 °C, and the supernatant containing cytoplasmic fractions was removed. B2 buffer (10 mM HEPES pH 7.5, 1% NP-40, 10 mM KCl, 1 mM $MgCl_2$, 400 mM NaCl, 20% glycerol, 0.5 mM EDTA pH 7.5, 0.1 mM EGTA pH 7.5, and 0.5 mM DTT) with protease and phosphatase inhibitors was added to pellets, mixed by shaker for 15 min at 4 °C. The lysate was further centrifuged at 10 600 ***g*** for 15 min at 4 °C, and the supernatant containing nuclear fractions was obtained and subjected to immunoblotting.

Mice

Five-week-old male wild-type (WT) C57BL/6J mice were purchased from Janvier (Le Genest-St-Isle, France). Mice were bred in the specific pathogen-free (SPF) facilities of Pasteur Institute, Lille. Mice were housed for 14 days prior to the experiment for the adaptations. Mice were housed under SPF conditions in individually ventilated cages in accordance with the national guidelines and regulations for the care and use of laboratory animals. Animal protocols were approved by the ethical committee of Ghent University (EC2019-024). Seven-week-old wild-type (WT) C57BL/6J mice were fed *ad libitum* with an AIN-93G diet (Research Diets, Inc., New Brunswick, NJ, USA) with or without 100 $mg \cdot kg^{-1}$ of (+)-cis, trans-Abscisic acid (A-050, Goldbio, St Louis, MO, USA) for 7 days.

Extraction of ABA and detection of ABA by LC–MS (Vion IMS QTof mass spectrometer analysis)

To determine ABA levels in serum, blood was collected from the heart ventricle and first incubated at room temperature for 30 min to allow the blood clot, followed by centrifugation at 1700 ***g*** for 10 min to separate the serum from the whole blood. Next, 200 μL of mice serum was added to 800 μL of methanol. The mixture was vortexed and incubated overnight at −70 °C in an ultrafreezer. The mixture was further centrifuged at 10 600 ***g*** for 15 min at 4 °C, and the supernatant was evaporated using a SpeedVac. The dried residue was resuspended in 1 mL of a 50 : 50 water:cyclohexane solution. The phases were separated by centrifugation at 10 600 ***g*** for 5 min. Next, 250 μL of 5% trichloroacetic acid was added to the collected aqueous phase and mixed by vortexing. The mixtures were partitioned three times against 500 μL of ethyl acetate, and the organic layer was collected and evaporated using a SpeedVac. The dried residue was resuspended in 50 μL of ultrapure water and filtered using an AcroPrep Advance 96-filter plate 0.2 μm Supor (Pall Life Sciences, Port Washington, NY, USA) prior to chromatographic separation and quantification by LC–MS/MS.

A 10 μL of the sample was injected on an ACQUITY UPLC BEH C18 (50 × 2.1 mm, 1.7 μm) column from Waters, and the temperature was maintained at 40 °C. A gradient of two buffers was used for separation: buffer A (99 : 1 : 0.1 water : acetonitrile : formic acid, pH 3) and buffer B (99 : 1 : 0.1 acetonitrile : water : formic acid, pH 3), as follows: 99% A for 0.1 min decreased to 50% A in 5 min, decreased to 30% from 5 to 7 min, and decreased to 0% from 7 to 10 min. The flow rate was set to 0.5 $mL \cdot min^{-1}$. The LockSpray ion source was operated in negative electrospray ionization mode under the following specific conditions: capillary voltage, 3.5 kV; reference capillary voltage, 2.5 kV; source temperature, 120 °C; desolvation gas temperature, 600 °C; desolvation gas flow,

1000 $L \cdot h^{-1}$; and cone gas flow, 50 $L \cdot h^{-1}$. The collision energy for the full MS scan was set at 6 eV. Mass range was set from 200 to 400 Da, and scan time was set at 1 s. Nitrogen (> 99.5%) was employed as desolvation and cone gas. Leucine-enkephalin [250 $pg \cdot \mu L^{-1}$ solubilized in water: acetonitrile 1 : 1 (v/v), with 0.1% formic acid] was used for the lock mass calibration, with scanning every 2 min at a scan time of 0.1 s. For multiple reaction monitoring purposes, precursor m/z and product m/z were set both at 263.13, collision energy was set at 6 eV, scan time was set on automatic, and capillary voltage was set at 3.5 kV. Profile data was recorded through UNIFI WORKSTATION v2.0 (Waters, Milford, MA, USA).

Statistical analysis

Statistical calculations were performed using SIGMAPLOT 12.0 (Jandel Scientific, San Jose, CA, USA) software. After testing data for normality (Shapiro–Wilk) and equal variance (Brown-Forsythe), the appropriate statistical tests (one-way ANOVA and the Home-Sidak's multiple comparisons test) were performed to determine a significant difference.

Acknowledgements

We thank BCCM/GeneCorner for storage and plasmid information infrastructure. Annick Bleys is acknowledged for critically reading the manuscript and text editing. We thank Dr Yasushi Todoroki (Shizouka University) for providing CYP707A inhibitor Abscinazole-E3M. SWK holds a scholarship from the VIB International PhD Program, FvG holds a scholarship from the Fund for Scientific Research-Flanders (FWO) (1SE0521N). The work was financially supported by an FWO grant (G021119N) and a Ghent University Concerted actions (GOA) grant (BOF19-GOA-004).

Conflict of interest

The authors declare that the research was conducted in the absence of any commercial or financial relationships that could be construed as a potential conflict of interest.

Author contributions

SWK: Methodology, Validation, Formal analysis, Investigation, Writing – Original Draft, Visualization. FVG: Methodology, Validation, Investigation, Writing – Review & Editing. KA: Methodology. YD: Validation. AG: Writing – Review & Editing, Supervision, Project administration. RB: Writing – Review & Editing, Supervision, Project administration, Funding acquisition. JS: Conceptualization, Methodology, Investigation, Writing – Review & Editing, Supervision, Project administration, Funding acquisition.

Data accessibility

The data that support the findings of this study are available from the corresponding author jens.staal@irc.vib-ugent.be upon reasonable request.

References

1 Jones AM, Danielson JÅ, ManojKumar SN, Lanquar V, Grossmann G, Frommer WB. Abscisic acid dynamics in roots detected with genetically encoded FRET sensors. *eLife*. 2014;**3**:e01741.
2 Waadt R, Hitomi K, Nishimura N, Hitomi C, Adams SR, Getzoff ED, et al. FRET-based reporters for the direct visualization of abscisic acid concentration changes and distribution in Arabidopsis. *eLife*. 2014;**3**:e01739.
3 Balcerowicz M, Shetty KN, Jones AM. Fluorescent biosensors illuminating plant hormone research. *Plant Physiol*. 2021;**187**:590–602.
4 Wu R, Duan L, Pruneda-Paz JL, Oh D, Pound M, Kay S, et al. The 6xABRE synthetic promoter enables the spatiotemporal analysis of ABA-mediated transcriptional Regulation1[OPEN]. *Plant Physiol*. 2018;**177**:1650–65.
5 Zhang L, Takahashi Y, Hsu P-K, Kollist H, Merilo E, Krysan PJ, et al. FRET kinase sensor development reveals SnRK2/OST1 activation by ABA but not by MeJA and high CO2 during stomatal closure. *eLife*. 2020;**9**:e56351.
6 Guri AJ, Hontecillas R, Si H, Liu D, Bassaganya-Riera J. Dietary abscisic acid ameliorates glucose tolerance and obesity-related inflammation in db/db mice fed high-fat diets. *Clin Nutr*. 2007;**26**:107–16.
7 Leber A, Hontecillas R, Tubau-Juni N, Zoccoli-Rodriguez V, Goodpaster B, Bassaganya-Riera J. Abscisic acid enriched fig extract promotes insulin sensitivity by decreasing systemic inflammation and activating LANCL2 in skeletal muscle. *Sci Rep*. 2020;**10**:10463.
8 Derosa G, Maffioli P, D'Angelo A, Preti PS, Tenore G, Novellino E. Abscisic acid treatment in patients with prediabetes. *Nutrients*. 2020;**12**:E2931.
9 Magnone M, Emionite L, Guida L, Vigliarolo T, Sturla L, Spinelli S, et al. Insulin-independent stimulation of skeletal muscle glucose uptake by low-dose abscisic acid via AMPK activation. *Sci Rep*. 2020;**10**:1454.
10 Guri AJ, Hontecillas R, Bassaganya-Riera J. Abscisic acid synergizes with rosiglitazone to improve glucose

tolerance and down-modulate macrophage accumulation in adipose tissue: possible action of the cAMP/PKA/PPAR γ axis. *Clin Nutr*. 2010;**29**:646–53.
11 Guri AJ, Hontecillas R, Bassaganya-Riera J. Abscisic acid ameliorates experimental IBD by downregulating cellular adhesion molecule expression and suppressing immune cell infiltration. *Clin Nutr*. 2010;**29**:824–31.
12 Guri AJ, Evans NP, Hontecillas R, Bassaganya-Riera J. T cell PPAR γ is required for the anti-inflammatory efficacy of abscisic acid against experimental IBD. *J Nutr Biochem*. 2011;**22**:812–9.
13 Qi C-C, Shu Y-M, Chen F-H, Ding Y-Q, Zhou J-N. Sensitivity during the forced swim test is a key factor in evaluating the antidepressant effects of abscisic acid in mice. *Behav Brain Res*. 2016;**300**:106–13.
14 Qi C-C, Zhang Z, Fang H, Liu J, Zhou N, Ge J-F, et al. Antidepressant effects of abscisic acid mediated by the downregulation of corticotrophin-releasing hormone gene expression in rats. *Int J Neuropsychopharmacol*. 2014;**18**:pyu006.
15 Sánchez-Sarasúa S, Moustafa S, García-Avilés Á, López-Climent MF, Gómez-Cadenas A, Olucha-Bordonau FE, et al. The effect of abscisic acid chronic treatment on neuroinflammatory markers and memory in a rat model of high-fat diet induced neuroinflammation. *Nutr Metab*. 2016;**13**:73.
16 Khorasani A, Abbasnejad M, Esmaeili-Mahani S. Phytohormone abscisic acid ameliorates cognitive impairments in streptozotocin-induced rat model of Alzheimer's disease through PPARβ/δ and PKA signaling. *Int J Neurosci*. 2019;**129**:1053–65.
17 Hoang QTM, Nguyen VK, Oberacher H, Fuchs D, Hernandez-Vargas EA, Borucki K, et al. Serum concentration of the phytohormone abscisic acid is associated with immune-regulatory mediators and is a potential biomarker of disease severity in chronic obstructive pulmonary disease. *Front Med*. 2021;**8**:693.
18 Zhou N, Yao Y, Ye H, Zhu W, Chen L, Mao Y. Abscisic-acid-induced cellular apoptosis and differentiation in glioma via the retinoid acid signaling pathway. *Int J Cancer*. 2016;**138**:1947–58.
19 Fresia C, Vigliarolo T, Guida L, Booz V, Bruzzone S, Sturla L, et al. G-protein coupling and nuclear translocation of the human abscisic acid receptor LANCL2. *Sci Rep*. 2016;**6**:26658.
20 Bassaganya-Riera J, Guri AJ, Lu P, Climent M, Carbo A, Sobral BW, et al. Abscisic acid regulates inflammation via ligand-binding domain-independent activation of peroxisome proliferator-activated receptor γ. *J Biol Chem*. 2011;**286**:2504–16.
21 Guri AJ, Hontecillas R, Ferrer G, Casagran O, Wankhade U, Noble AM, et al. Loss of PPARγ in immune cells impairs the ability of abscisic acid to improve insulin sensitivity by suppressing monocyte chemoattractant protein-1 expression and macrophage infiltration into white adipose tissue. *J Nutr Biochem*. 2008;**19**:216–28.
22 Hontecillas R, Roberts PC, Carbo A, Vives C, Horne WT, Genis S, et al. Dietary abscisic acid ameliorates influenza-virus-associated disease and pulmonary immunopathology through a PPARγ-dependent mechanism. *J Nutr Biochem*. 2013;**24**:1019–27.
23 Sommer M, Wolf G. Rosiglitazone increases PPARgamma in renal tubular epithelial cells and protects against damage by hydrogen peroxide. *Am J Nephrol*. 2007;**27**:425–34.
24 Dutta D, Lai K-Y, Reyes-Ordoñez A, Chen J, van der Donk WA. Lanthionine synthetase C-like protein 2 (LanCL2) is important for adipogenic differentiation. *J Lipid Res*. 2018;**59**:1433–45.
25 Bruzzone S, Moreschi I, Usai C, Guida L, Damonte G, Salis A, et al. Abscisic acid is an endogenous cytokine in human granulocytes with cyclic ADP-ribose as second messenger. *Proc Natl Acad Sci USA*. 2007;**104**:5759–64.
26 Magnone M, Sturla L, Jacchetti E, Scarfì S, Bruzzone S, Usai C, et al. Autocrine abscisic acid plays a key role in quartz-induced macrophage activation. *FASEB J*. 2012;**26**:1261–71.
27 Le Page-Degivry M-T, Bidard J, Rouvier E, Bulard C, Lazdunski M. Presence of abscisic acid, a phytohormone, in the mammalian brain. *Proc Natl Acad Sci USA*. 1986;**83**:1155–8.
28 Bruzzone S, Basile G, Mannino E, Sturla L, Magnone M, Grozio A, et al. Autocrine abscisic acid mediates the UV-B-induced inflammatory response in human granulocytes and keratinocytes. *J Cell Physiol*. 2012;**227**:2502–10.
29 Sakamoto S, Putalun W, Vimolmangkang S, Phoolcharoen W, Shoyama Y, Tanaka H, et al. Enzyme-linked immunosorbent assay for the quantitative/qualitative analysis of plant secondary metabolites. *J Nat Med*. 2018;**72**:32–42.
30 Su Y, Li W, Huang Z, Wang R, Luo W, Liu Q, et al. Sensitive and high throughput quantification of abscisic acid based on quantitative real time immuno-PCR. *Plant Methods*. 2018;**14**:104.
31 Liang F-S, Ho WQ, Crabtree GR. Engineering the ABA Plant stress pathway for regulation of induced proximity. *Sci Signal*. 2011;**4**:rs2.
32 Lebar T, Lainšček D, Merljak E, Aupič J, Jerala R. A tunable orthogonal coiled-coil interaction toolbox for engineering mammalian cells. *Nat Chem Biol*. 2020;**16**:513–9.
33 Dupeux F, Santiago J, Betz K, Twycross J, Park S-Y, Rodriguez L, et al. A thermodynamic switch modulates abscisic acid receptor sensitivity: a thermodynamic switch in the ABA pathway. *EMBO J*. 2011;**30**:4171–84.
34 Lievens L, Pollier J, Goossens A, Beyaert R, Staal J. Abscisic acid as pathogen effector and immune regulator. *Front Plant Sci*. 2017;**8**:587.

35 Miyazono K, Miyakawa T, Sawano Y, Kubota K, Kang H-J, Asano A, et al. Structural basis of abscisic acid signalling. *Nature*. 2009;**462**:609–14.
36 Szostkiewicz I, Richter K, Kepka M, Demmel S, Ma Y, Korte A, et al. Closely related receptor complexes differ in their ABA selectivity and sensitivity. *Plant J*. 2010;**61**:25–35.
37 Santiago J, Rodrigues A, Saez A, Rubio S, Antoni R, Dupeux F, et al. Modulation of drought resistance by the abscisic acid receptor PYL5 through inhibition of clade a PP2Cs. *Plant J*. 2009;**60**:575–88.
38 Kushiro T, Okamoto M, Nakabayashi K, Yamagishi K, Kitamura S, Asami T, et al. The Arabidopsis cytochrome P450 CYP707A encodes ABA 8′-hydroxylases: key enzymes in ABA catabolism. *EMBO J*. 2004;**23**:1647–56.
39 Saito S, Hirai N, Matsumoto C, Ohigashi H, Ohta D, Sakata K, et al. Arabidopsis CYP707As encode (+)-abscisic acid 8′-hydroxylase, a key enzyme in the oxidative catabolism of abscisic acid. *Plant Physiol*. 2004;**134**:1439–49.
40 Talmann L, Wiesner J, Vilcinskas A. Strategies for the construction of insect P450 fusion enzymes. *Z Naturforsch C J Biosci*. 2017;**72**:405–15.
41 Artsaenko O, Peisker M, Zur Nieden U, Fiedler U, Weiler EW, Müntz K, et al. Expression of a single-chain Fv antibody against abscisic acid creates a wilty phenotype in transgenic tobacco. *Plant J*. 1995;**8**:745–50.
42 Xiong D-M, Liu Z, Chen H, Xue J-T, Yang Y, Chen C, et al. Profiling the dynamics of abscisic acid and ABA-glucose ester after using the glucosyltransferase UGT71C5 to mediate abscisic acid homeostasis in *Arabidopsis thaliana* by HPLC–ESI-MS/MS. *J Pharm Anal*. 2014;**4**:190–6.
43 Lin Y-C, Boone M, Meuris L, Lemmens I, Van Roy N, Soete A, et al. Genome dynamics of the human embryonic kidney 293 lineage in response to cell biology manipulations. *Nat Commun*. 2014;**5**:4767.
44 Sturla L, Fresia C, Guida L, Bruzzone S, Scarfì S, Usai C, et al. LANCL2 is necessary for abscisic acid binding and signaling in human granulocytes and in rat insulinoma cells. *J Biol Chem*. 2009;**284**:28045–57.
45 Chan LSA, Wells RA. Cross-talk between PPARs and the partners of RXR: a molecular perspective. *PPAR Res*. 2009;**2009**:925309.
46 le Maire A, Teyssier C, Balaguer P, Bourguet W, Germain P. Regulation of RXR-RAR heterodimers by RXR- and RAR-specific ligands and their combinations. *Cell*. 2019;**8**:1392.
47 Bruzzone S, Bodrato N, Usai C, Guida L, Moreschi I, Nano R, et al. Abscisic acid is an endogenous stimulator of insulin release from human pancreatic islets with cyclic ADP ribose as second messenger. *J Biol Chem*. 2008;**283**:32188–97.
48 Bruzzone S, Ameri P, Briatore L, Mannino E, Basile G, Andraghetti G, et al. The plant hormone abscisic acid increases in human plasma after hyperglycemia and stimulates glucose consumption by adipocytes and myoblasts. *FASEB J*. 2012;**26**:1251–60.
49 Miyazaki S, Tashiro F, Tsuchiya T, Sasaki K, Miyazaki J-I. Establishment of a long-term stable β-cell line and its application to analyze the effect of Gcg expression on insulin secretion. *Sci Rep*. 2021;**11**:477.
50 Shi J, Fan J, Su Q, Yang Z. Cytokines and abnormal glucose and lipid metabolism. *Front Endocrinol*. 2019;**10**:703.
51 Yang X, Boehm JS, Yang X, Salehi-Ashtiani K, Hao T, Shen Y, et al. A public genome-scale lentiviral expression library of human ORFs. *Nat Methods*. 2011;**8**:659–61.
52 Zeng M, van der Donk WA, Chen J. Lanthionine synthetase C–like protein 2 (LanCL2) is a novel regulator of Akt. *Mol Biol Cell*. 2014;**25**:3954–61.
53 De Groote P, Grootjans S, Lippens S, Eichperger C, Leurs K, Kahr I, et al. Generation of a new gateway-compatible inducible lentiviral vector platform allowing easy derivation of co-transduced cells. *Biotechniques*. 2016;**60**:252–9.
54 Schmitz ML, Baeuerle PA. The p65 subunit is responsible for the strong transcription activating potential of NF-kappa B. *EMBO J*. 1991;**10**:3805–17.
55 Petersen LK, Stowers RS. A gateway MultiSite recombination cloning toolkit. *PLoS ONE*. 2011;**6**: e24531.
56 Ishida T, Mizushima S i, Azuma S, Kobayashi N, Tojo T, Suzuki K, Aizawa S, Watanabe T, Mosialos G, Kieff E, Yamamoto T & Inoue J (1996) Identification of TRAF6, a novel tumor necrosis factor receptor-associated factor protein that mediates signaling from an amino-terminal domain of the CD40 cytoplasmic region. *J Biol Chem* **271**, 28745–28748.